buildings

MDPI

Article

Seismic Fragility and Loss Assessment of a Multi-Story Steel Frame with Viscous Damper in a Corrosion Environment

Wenwen Qiu [1,2], Haibo Wen [3,*], Chenhui Gong [4], Zhenkai Zhang [1], Wenjing Li [1] and Shuo Li [1]

[1] School of Economics and Management, Gandong University, Fuzhou 344000, China; wenwenqiu@gdc.edu.cn (W.Q.); zhenkaizhang@gdc.edu.cn (Z.Z.); wenjingli@gdc.edu.cn (W.L.); shuoli@gdc.edu.cn (S.L.)
[2] School of Business Management, University Utara Malaysia, Sintok 06010, Kedah, Malaysia
[3] School of Civil Engineering, Central South University, Changsha 410075, China
[4] School of Applied Engineering, Gandong University, Fuzhou 344000, China; chenhuigong@gdc.edu.cn
* Correspondence: haibowen_2000@163.com

Abstract

Corrosion can accelerate the deterioration of the mechanical properties of steel structures. However, few studies have systematically evaluated its impact on seismic performance, particularly with respect to seismic economic losses. In this paper, the seismic fragility and loss assessment of a multi-story steel frame with viscous dampers (SFVD) building are investigated through experimental and numerical analysis. Based on corrosion and tensile test results, OpenSees software 3.3.0 was used to model the SFVD, and the effect of corrosion on the seismic fragility was evaluated via incremental dynamic analysis (IDA). Then, the economic losses of the SFVD during different seismic intensities were assessed at various corrosion times based on fragility analysis. The results show that as the corrosion time increases, the mass and cross-section loss rate of steel increase, causing a decrease in mechanical property indices, and theprobability of exceedance of the SFVD in the limit state increases gradually with increasing corrosion time, with an especially significant impact on the collapse prevention (CP) state. Furthermore, the economic loss assessment based on fragility curves indicates that the economic loss increases with corrosion time. Thus, the aim of this paper is to provide guidance for the seismic design and risk management of steel frame buildings in coastal regions throughout their life cycle.

Keywords: steel frame; corrosion; seismic fragility; loss assessment

check for updates

Academic Editor: Harry Far

Received: 15 May 2025
Revised: 20 June 2025
Accepted: 12 July 2025
Published: 17 July 2025

Citation: Qiu, W.; Wen, H.; Gong, C.; Zhang, Z.; Li, W.; Li, S. Seismic Fragility and Loss Assessment of a Multi-Story Steel Frame with Viscous Damper in a Corrosion Environment. *Buildings* **2025**, *15*, 2515. https://doi.org/10.3390/buildings15142515

Copyright: © 2025 by the authors. Licensee MDPI, Basel, Switzerland. This article is an open access article distributed under the terms and conditions of the Creative Commons Attribution (CC BY) license (https://creativecommons.org/licenses/by/4.0/).

1. Introduction

Steel structures have been extensively employed in modern construction due to their high strength, excellent ductility, and easy construction [1,2]. However, traditional steel frames exhibit relatively low lateral stiffness and insufficient ductility capacity, particularly in high-rise buildings, leading to challenges in meeting practical seismic performance requirements. The equipment of structural dampers [3,4] serves as an effective seismic retrofitting measure, significantly enhancing the seismic performance of steel frames and reducing their seismic-induced responses.

Steel buildings are prone to corrosion in humid or other corrosive environments, which degrades their mechanical properties, thereby affecting the overall safety and seismic performance of the structure. Salt spray corrosion is one of the main types of corrosion that steel buildings face in coastal areas, and chloride ions can accelerate the corrosion process of steel [5]. Corrosion has no significant effect on the mechanical or chemical properties of

steel, and the degradation of mechanical properties is attributed mainly to the reduction in steel section thickness caused by corrosion [6]. Guo et al. [7] investigated the mechanical behavior of Q345 steel after long-term corrosion in a salt spray environment and observed a decrease in yield strength, ultimate strength, and fracture strength with increasing corrosion degree (mass loss rate η), especially when $\eta \geq 10\%$. Corrosion affects different steel types in various ways. Kong et al. [8] analyzed the corrosion products and microstructures of Q235 and Q355 steels after corrosion using XRD and SEM, and the results showed that although the corrosion products of both steels were similar, their microstructural morphologies differed significantly. Compared to Q235 steel, corrosion has a smaller effect on the strength and ductility of Q355 steel. Furthermore, corrosion weakens the fatigue strength of steel, with this effect being more pronounced at high temperatures [9,10].

In recent years, numerous studies have evaluated the effect of corrosion on the seismic performance of steel structures from the perspective of steel structures and steel members, and the results showed that corrosion can reduce the load-carrying capacity, deformation capacity, and energy-dissipation capacity of steel frames [11–14]. Zhang et al. [12] investigated the seismic performance of steel beam-to-column connections after corrosion, and the results showed that corrosion lowers the load-bearing capacity, initial stiffness and energy-dissipation capacity of steel beam-column connections and accelerates local buckling. Zhang et al. [14] investigated the effect of corrosion on the seismic behavior of steel frames using experiments and finite element analysis, quantified the corrosion level with the mass loss rate and developed a deterioration model for the mechanical properties of steel as corrosion increases. Therefore, it is worthwhile to investigate the seismic performance of corrosion on steel frames.

Seismic fragility, defined as the probability that a structure will reach or exceed a specific damage index, is crucial for assessing a structure's seismic performance. Lad et al. [15] used IDA to assess the seismic fragility of corroded steel frames and local components and reported that corrosion reduces the load-bearing and energy-dissipation capacity of steel frames, increasing their damage probability during earthquakes. Notably, corrosion most significantly affects the fragility of columns. Xu et al. [16] performed accelerated corrosion tests on a 5-story steel frame and used IDA to obtain seismic fragility curves under various corrosion times, and the results showed that the structure's probability of exceedance gradually increases with increasing corrosion time, with the most significant impact observed on the CP state. Lekeufack et al. [17] analyzed the fragility curves of three kinds of steel frames (NCSF, CCSF, and CWSF) under various seismic intensities, and the results showed that corrosion significantly increases structural fragility. Moreover, CWSF shows lower fragility than CCSF, particularly in the CP state. Additionally, assessing seismic-induced economic losses via fragility or fragility functions is effective. For example, Jiang et al. [18] considered the uncertainty between failure probability and damage cost, proposed a cost-based seismic fragility analysis method, and calculated the seismic life cycle cost of steel frames with steel plate walls. Significant endeavors have been witnessed to quantify the effects of corrosion on the seismic performance and seismic fragility of steel frames. However, few studies are related to the influence of corrosion on seismic loss assessment. In addition, although many studies have evaluated the seismic life cycle cost of steel frames, the effect of natural corrosion has not been considered.

To this end, this paper attempts to investigate the effect of corrosion on the fragility and economic loss of a multi-story SFVD for potential use in the seismic design and risk management of steel frame buildings in coastal regions throughout their life cycle. The difference between the present investigation and other studies is that it takes into account the impact of corrosion on the fragility of steel frame structures and establishes a link between corrosion and economic losses via fragility analysis.

2. Experimental Study on Steel Corrosion

2.1. Materials

The material used for the corrosion test in this work was Q355 construction steel. Specimens were designed according to Chinese standard GB/T228.1-2010 [19] and GB/3075-2008 [20]. The specimen thickness was 18 mm, as shown in Figure 1.

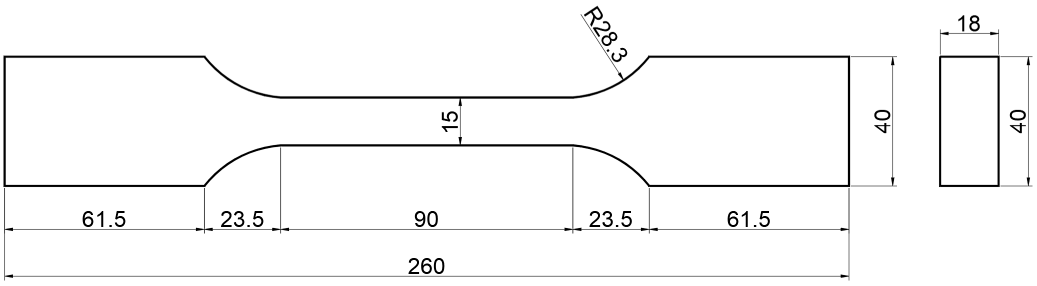


Figure 1. Specimen dimensions (unit: mm).

2.2. Corrosion Test

In this paper, an artificial spray accelerated corrosion test was conducted on Q355 construction steel. According to References [7,16], the corrosion tests were carried out at a room temperature of 25 °C and a relative humidity of 44%, and the corrosive solution used was a 50 g/L NaCl solution with a pH of 6.5–7.5. To ensure uniform corrosion on both sides of the specimens, they were fixed at a 45° angle to the horizontal plane. The spray method used was an intermittent spray with a 1-day cycle, and all specimens were flipped every eight days. Prior to the experiment, a 10% oxalic acid solution was prepared, and the processed specimens were ultrasonically cleaned to remove surface oils and residues, followed by drying. After the experiment, rust was removed from the specimens via a 20% oxalic acid solution. The specimens were subsequently neutralized with a 20% sodium carbonate solution, dried, weighed, and stored in plastic bags.

After corrosion, the specimens were numbered and grouped according to the corrosion time (32, 64, 92, 128, 164, and 192 days) into six groups, with three specimens per group to reduce randomness. They were labeled in the form of Si (i = 0, 1, 2. . .18). Among them, S0 represents the uncorroded specimen, and S1, S2, and S3 denote the three groups of specimens corroded for 32 days, and so on.

2.3. Tensile Test

To investigate the mechanical properties of steel at various corrosion times, tensile tests were conducted on both corroded and uncorroded specimens via a T-shaped working test bench. A total of 19 groups of tests were carried out, as shown in Figure 2. In accordance with the Chinese standard GB/T 228.1 [19], tensile tests were performed on corroded specimens via displacement control. The loading rates for the elastic, yield, and strain-hardening stages were 1.3 mm/min, 1.3 mm/min, and 10.8 mm/min, respectively.

Prior to the experiment, to measure the elongation of the corroded steels, a gauge length of 90 mm was used to mark the tensile section of each specimen. After fracture, the final length within the gauge region was measured via a digital Vernier caliper. In addition, during the test, the average thickness and width of each specimen were input to obtain the mechanical properties of the steel.



Figure 2. T-shaped working test bench.

2.4. Results

Here, the mass loss η and cross-section loss rate η_s of specimens at various corrosion times were analyzed, which can be expressed as follows:

$$\eta = \frac{W_0 - W_1}{W_0} \times 100\% \quad (1)$$

$$\eta_s = \frac{A_0 - A_1}{A_0} \times 100\% \quad (2)$$

where W_0 and W_1 are the mass of the specimen before and after corrosion, respectively; A_0 and A_1 are the initial area and residual area of the specimen before and after corrosion, respectively.

Figure 3 shows the relationship between the mass loss rate and corrosion time of the specimens, where the scatter points represent the experimental results and the solid line represents the fitting result. The results show that the mass loss rate gradually increases with increasing corrosion time. Compared with the uncorroded specimens, the mass loss rate of the specimens after 192 days of corrosion decreases by a maximum of 11.00%. It is worth noting that the mass loss rate shows a significant power-function [7] relationship with corrosion time, with a correlation coefficient exceeding 99%. In addition, comparing the mass loss rates of specimens at the same age reveals small numerical differences, which suggests uniform corrosion.

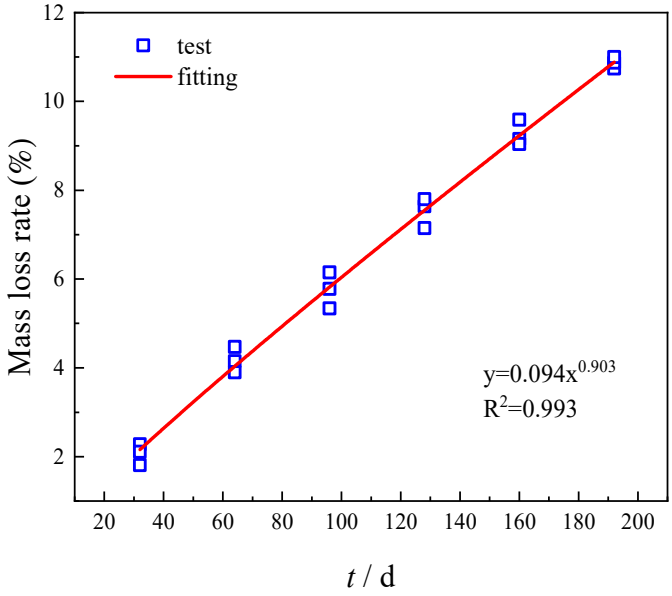


Figure 3. Mass loss rate for various corrosion times.

Figure 4 shows the cross-section loss rate at various corrosion times. The results show that the cross-section loss rate increases with increasing corrosion time, and the cross-section loss rate has a strong linear relationship with corrosion time.

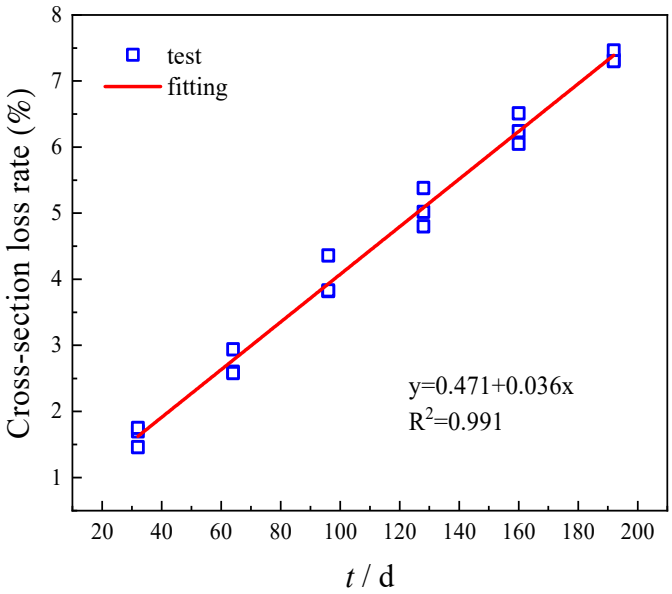


Figure 4. Cross-section loss rate for various corrosion times.

Common parameters used to characterize the degree of steel corrosion include mass loss rate, cross-section loss rate, and corrosion time. However, due to variations in testing methods and specimen dimensions among different corrosion tests, these parameters cannot be directly compared. Here, a relationship between mass loss rate, cross-section loss rate, and corrosion time was established, which can predict corrosion degree parameters at different corrosion times and provide a reference for conversion.

Figure 5 shows the nominal stress–strain curves of the corroded specimens after the tensile test. The results show that with increasing corrosion, the yield strength, ultimate tensile strength, and elongation of the steel all exhibit a downward trend, which is mainly attributed to the formation of rust pits on the steel surface due to corrosion, thereby

reducing the effective cross-sectional area of the steel [6,21]. In the elastic stage, the stress–strain curves of all the corroded specimens are highly similar, indicating that corrosion has little effect on the elastic modulus of steel. Additionally, the corroded specimens show no distinct yield plateau, a phenomenon that may be due to the excessive carbon content in the steel during processing which reduces its ductility.

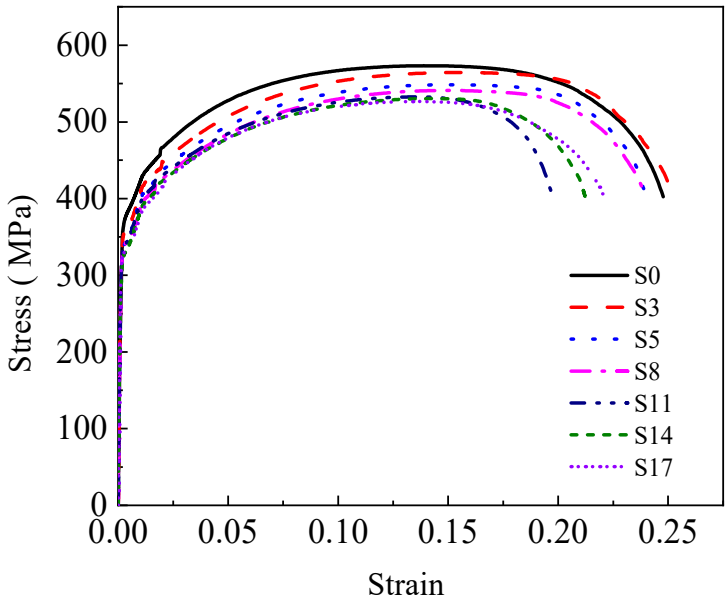


Figure 5. Stress–strain curve of the corrosion specimens.

It is well known that the rough surface of corroded steel can affect the accuracy of measuring the cross-sectional area of the parallel section. Hence, this work uses the nominal stress as the evaluation index. Table 1 shows the main parameters from the tensile test, including elastic modulus (E_s), yield strength (f_y), ultimate tensile strength (f_u), ultimate load (F_u), yield-strength ratio (f_y/f_u), and elongation (δ). In addition, owing to the lack of an obvious yield plateau in the corroded specimens, the conditional yield strength is used as the yield strength of the specimens here.

Table 1. Specimen mechanical property indices.

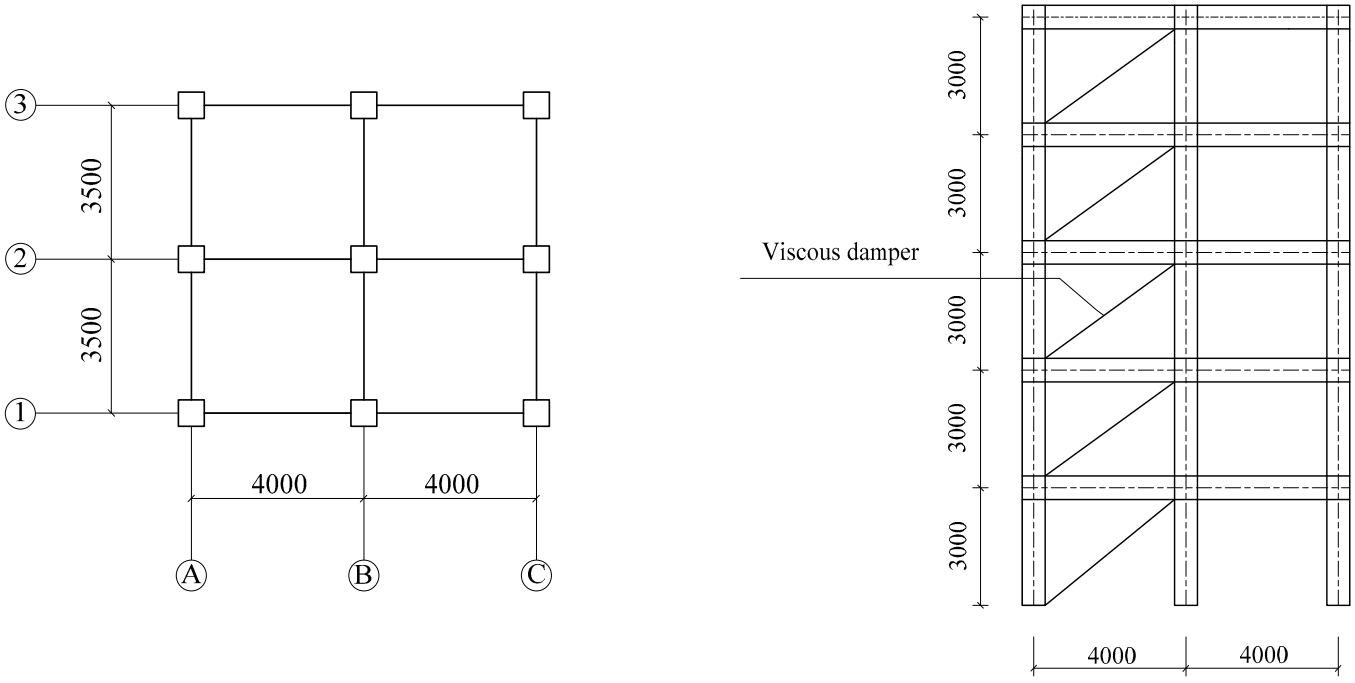
t/d	No.	E_s/MPa	f_y/*t*MPa	f_u/MPa	F_u/MPa	f_y/f_u	δ
0	S0	198.38	375.86	573.22	155.88	0.656	24.77%
	S4	188.63	347.26	551.43	146.06	0.630	23.20%
64	S5	187.66	342.39	548.45	144.76	0.624	24.01%
	S6	184.43	338.61	543.93	144.10	0.623	23.97%
	S10	183.33	339.59	538.61	139.44	0.630	19.82%
128	S11	183.87	339.62	532.68	137.06	0.638	19.74%
	S12	184.61	345.95	521.68	134.74	0.663	18.54%
	S16	— —	— —	— —	— —	— —	— —
192	S17	177.56	329.32	526.54	132.50	0.625	22.10%
	S18	179.45	332.30	532.11	134.14	0.625	20.16%

As shown in Table 1, all the indices of the corroded specimens decrease gradually with increasing corrosion time. Compared to the uncorroded specimen S0, the nominal elastic modulus, nominal yield strength, nominal tensile strength, and ultimate load of the S-series corroded specimens decrease by a maximum of 10.50%, 12.38%, 8.14%, and 15.00%, respectively. Furthermore, the elongation of steel decreases by up to 25.15% under the most severe corrosion, indicating that corrosion has a significant impact on the ductility

of steel. Although the yield-strength ratio of steel decreases, the trend is not remarkable. The ratio fluctuates around 0.63 for the S-series corroded specimens, which meets the Chinese standard GB/T 19879-2005 [22] with a value of less than 0.85. This suggests that the mechanical property degradation of corroded steel does not significantly affect its safe reserve capacity.

3. Fragility Analysis of the SFVD

In this paper, the OpenSees software was employed to model a 5-story, 2-span SFVD presented in reference [23], as shown in Figure 6. The X-direction and Y-direction spans of the steel frame are 4000 mm and 3500 mm, respectively, and each floor is 3000 mm high. The section size of the beams is H200 × 600 × 20 × 20, and the section size of the columns is H600 × 600 × 20 × 20. In addition, the viscous damper was installed on Axis 2 of the SFVD, as shown in Figure 6a, with a stiffness of 100 kN/mm, a damping coefficient of 3 kN(s/m), and a damping coefficient of 1.



(**a**) floor plan (**b**) elevation drawing

Figure 6. Schematic diagram of the SFVD (unit: mm).

In the modeling process, the mechanical parameters of the S-series steel with corrosion times of 0, 64, 128, and 192 days from Section 2 are used to predict the mechanical properties of the 5-story steel frame after corrosion. Frame columns are rigidly connected to the ground and frame beams, while viscous dampers adopt hinged connections; the simulation of viscous dampers employs Maxwell elements. Given that the SFVD model has been validated in reference [23], more details are not reiterated here.

3.1. Seismic Wave Selection

To determine the uncertainty of seismic hazards, it is generally necessary to select representative real-world seismic waves from a region for measurement. In this paper, 20 representative seismic ground motion records suitable for seismic analysis of regions such as Los Angeles, Boston, and Seattle in the United States were selected for IDA, which was based on a SAC project [24] funded by FEMA for steel structure design, as shown in

Figure 7. Here, the spectral acceleration $S_a(T_1)$ was adopted as the intensity measure (*IM*) in the IDA.

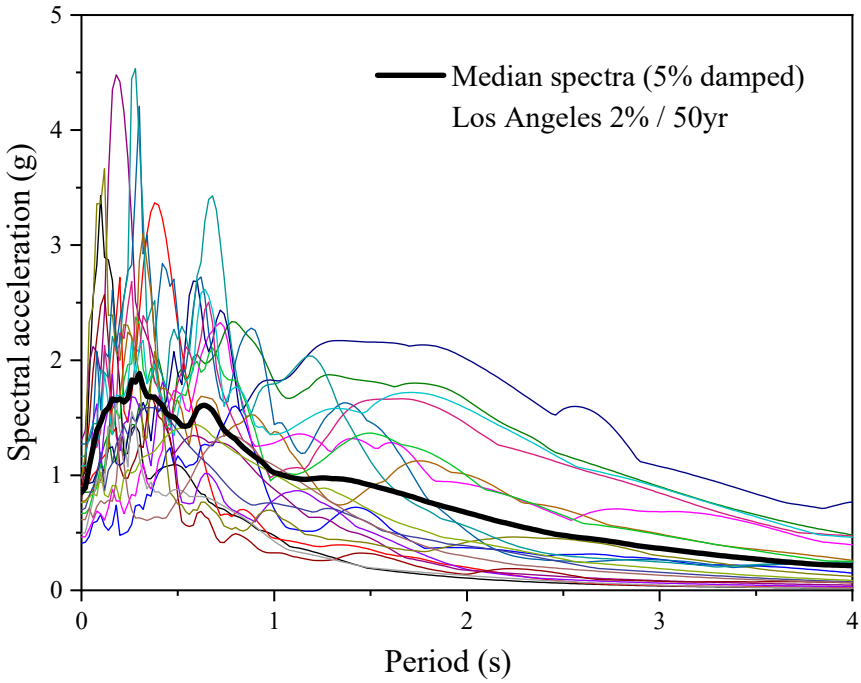


Figure 7. Response spectra of the 20 selected ground motions.

3.2. Determination of the Damage Measure

In this paper, the IDA method is employed to assess the seismic performance of the structure, which has the advantages [17,25] of capturing the complete range of the structural responses, accounting for uncertainties, and evaluating multiple limit states. The selection of the structural damage measure (*DM*) is critical prior to performing IDA analyses. Ye and Jiang et al. [26,27]. selected the maximum inter-story drift ratio as the *DM* and confirmed its reliability. In addition, the Chinese standard GB50010-2010 [28] specifies the maximum inter-story drift ratio as the threshold value for seismic deformation checking and proves that this parameter can be commonly used as a significant index for seismic design and performance evaluation. Therefore, in this paper, the maximum inter-story drift ratio is selected as the *DM* for the IDA of the SFVD. A brief description of the IDA process is as follows: IDA of the SFVD structure was performed using 20 selected ground motions from Figure 7, with $S_a(T_1)$ as the IM and scaled in increments of 0.25 g. The analysis was terminated when the maximum inter-story drift ratio reached 4%. The relationship between $S_a(T_1)$ and the maximum inter-story drift ratio was then obtained.

3.3. Determination of the Damage States

The Federal Emergency Management Agency (FEMA) defined structural damage into three levels [29]: immediate occupancy (IO), structural damage (SD) and collapse prevention (CP), as shown in Figure 8. These states divide structural performance into four levels: immediate occupancy, remaining operation, life-safety maintenance and near collapse. The current Chinese seismic design code defined structural damage into four levels: no damage, slight damage, moderate damage, and severe damage. The two classification approaches are highly consistent. Hence, in this paper, the maximum inter-story drift ratios for the IO, SD, and CP states are defined as 1%, 2%, and 4%, respectively.

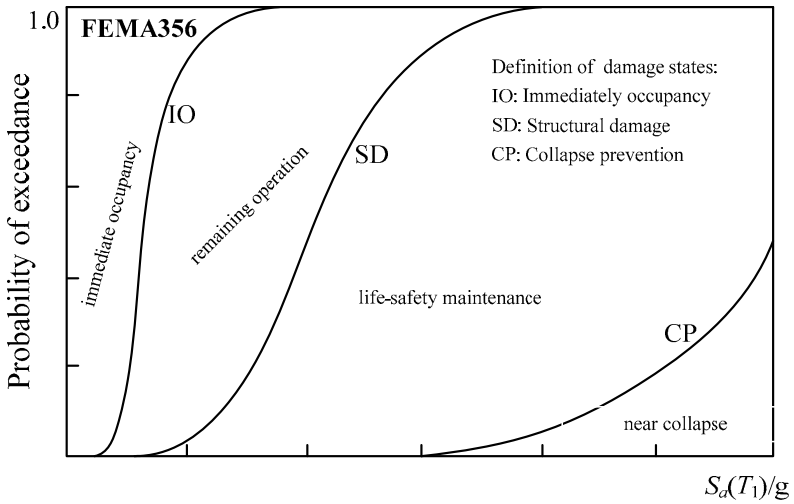


Figure 8. FEMA 356 definition of damage states.

3.4. Fragility Curve Analysis

The *IM* and *DM* follow a lognormal distribution, and their relationship is expressed as follows:

$$DM = \alpha(IM)^{\beta} \tag{3}$$

where α and β are coefficients determined by regression.

In this section, $S_a(T_1)$ and the maximum inter-story drift are selected as the *IM* and *DM*, respectively. The cloud method is employed to develop a linear relationship between θ_{max} and $S_a(T_1)$ on a log–log coordinate system, as shown in the following equation.

$$\ln \theta_{max} = a + \beta \ln[S_a(T_1)] \tag{4}$$

where $a = \ln \alpha$ is a constant.

According to the three damage states (IO, SD, and CP) of the 5-story SFVD building, the spectral acceleration of each state can be retrieved. Then, the logarithmic standard deviations of different random variables are calculated. The calculation formula is as follows:

$$\beta = \sqrt{\frac{\sum_{i=1}^{N} (\ln Sa_i - \ln m)^2}{N-2}} \tag{5}$$

where m and β are the median value and the logarithmic standard deviation of the seismic intensity in the fragility function, respectively. And N represents the number of input ground motion records.

According to Equation (5), the logarithmic standard deviations for each damage state at various corrosion times were calculated, as shown in Table 2. Here, the seismic fragility function based on seismic intensity measures is used to reflect the seismic fragility. This function follows a standard lognormal distribution, which can be expressed as follows:

$$F(x) = \varphi\left[\frac{(\ln x - \ln m)}{\beta}\right] \tag{6}$$

where $\varphi(*)$ represents the integral of the standard normal probability [30,31].

Table 2. Fragility parameters for various corrosion times.

Corrosion Time (d)		IO	SD	CP
		θ_{max} = 1%	θ_{max} = 2%	θ_{max} = 4%
0	m	1.1434035	2.286815	4.573625
	β	0.4282113	0.428214	0.428215
64	m	1.0984700	2.1969300	4.3938750
	β	0.4423005	0.4422966	0.4427271
128	m	1.0741750	2.1483550	4.2967100
	β	0.4431142	0.4431152	0.4431155
192	m	1.0574000	2.1148017	4.2296018
	β	0.4746999	0.4797504	0.4797512

According to Equation (6), the seismic fragility curves of the SFVD in the IO, SD, and CP performance limit states at various corrosion times can be obtained, as shown in Figure 9. The results show that the trend of the fragility curves remains essentially consistent across all corrosion times. Within the test seismic motion range, the probability of exceedance increases gradually with increasing $S_a(T_1)$, indicating an increase in the fragility of the SFVD.

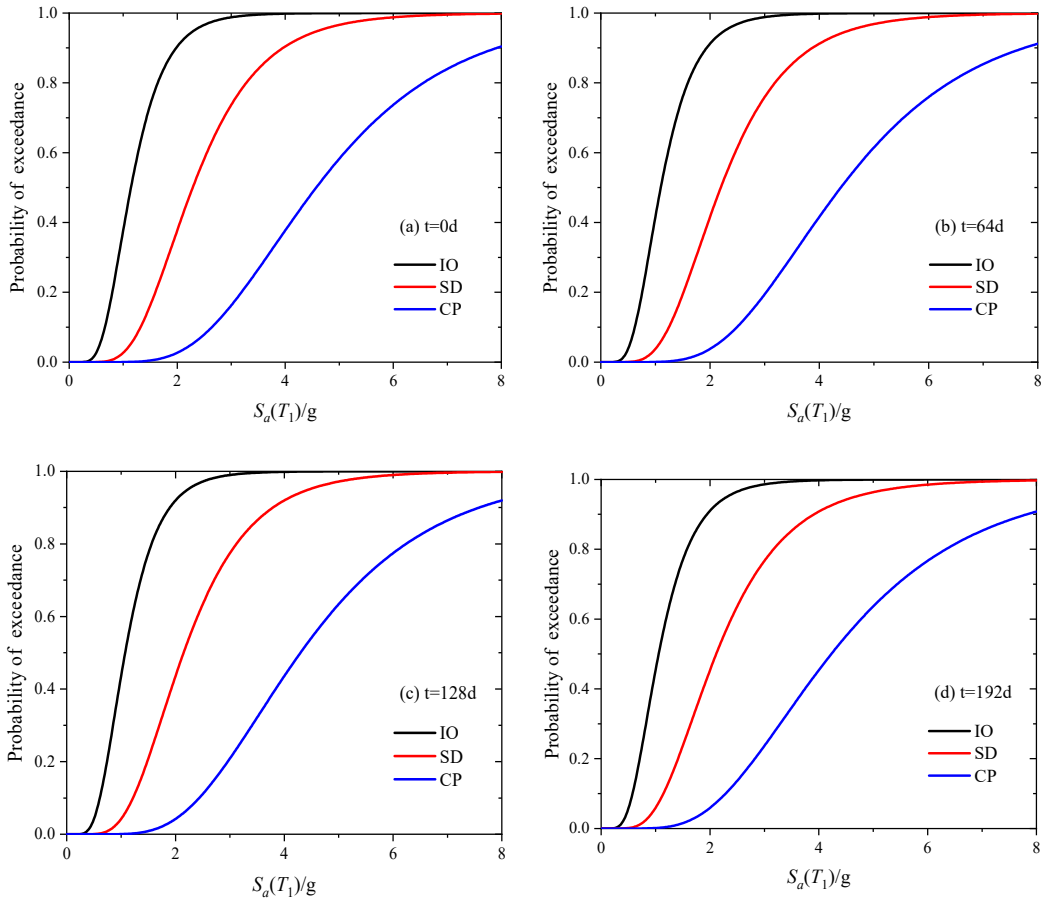


Figure 9. Fragility curves for various corrosion times: (**a**) 0 days; (**b**) 64 days; (**c**) 128 days; and (**d**) 192 days.

To gain a clearer understanding of the impact of corrosion time on fragility, all the results from Figure 8 are plotted on the same coordinate system, as shown in Figure 10. It is evident that at the same $S_a(T_1)$, the probability of exceedance gradually increases with increasing corrosion time, which is due to the fact that corrosion reduces the cross-sectional

area of structural components, thereby decreasing the seismic resistance of the SFVD. In addition, comparing the fragility curves in the three limit states, it is observed that the fragility curves in the IO and SD stated do not significantly change, whereas the curve for the CP state exhibits a more pronounced variation. For example, when the probability of exceedance is 50%, the corresponding differences in $S_a(T_1)$ between the SFVDs with 0 days and 192 days of corrosion are 0.08 g and 0.16 g for the IO and SD states, respectively, while this difference for the CP state reaches 0.35 g. From another perspective, when $S_a(T_1)$ is 3 g, compared to the uncorroded SFVD, the SFVD with 192 days of corrosion shows an increase of 7.46% in probability of exceedance in the CP state, and an increase of 3.00% in the SD state, while their probabilities in the IO state are nearly the same. This indicates that corrosion has an especially significant impact on the probability of exceedance of the SFVD in the CP state.

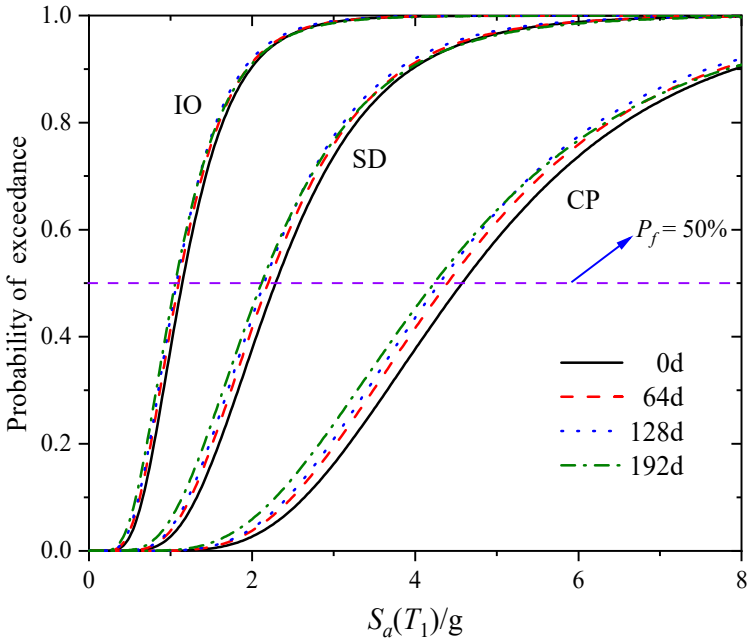


Figure 10. Comparison of fragility curves for various corrosion times.

4. Loss Assessment of the SFVD

4.1. Economic Losses

In the previous sections, the occurrence probabilities at various damage states (IO, SD, and CP) during different seismic intensities were obtained from performance-based fragility functions. Considering the impact of corrosion on seismic economic losses, this paper proposes a fragility analysis-based methodology for quantifying seismic-induced economic losses. By establishing a relationship between the probability of exceedance at different seismic intensities and corresponding economic losses, this method calculates the economic losses of buildings under various seismic intensity levels, offering a scientific basis for earthquake risk management and disaster prevention planning.

Seismic economic losses are generally comprised of the following three components: (1) direct economic losses encompassing structural damage to buildings and property losses; (2) indirect economic losses resulting from income disruption due to structural functional downtime; and (3) human casualty costs associated with injuries or fatalities. Silva et al. [32] and Nettis et al. [33] conducted a detailed assessment of the direct economic losses of buildings under earthquake action, establishing a relationship between economic losses and initial costs through damage factors. However, they neglected the contributions of building downtime and casualties. Here, the economic loss of steel frames is regarded as

the sum of the maintenance costs, the recovery costs of damaged equipment and accessories inside the building, compensation expenses for casualties, and costs related to revenue loss from other shutdowns. Moreover, considering that the earthquake occurrence probability varies with different damage states, $C_{seismic}$ can be expressed by the following equation:

$$C_{seismic} = \sum_{j=1}^{K} C_j P_j \tag{7}$$

where C_j and P_j represent the loss cost and occurrence probability of the jth damage state, C_j and P_j can be written as

$$C_j = C_j^{damage} + C_j^{content} + C_j^{relocation} + C_j^{economic} + C_j^{injury} + C_j^{fatality} \tag{8}$$

$$P_j = \begin{cases} 1 - P_1 \ (j = 1) \\ P_{j-1} - P_j \ (j = 2, 3) \\ P_4 \ \ (j = 4) \end{cases} \tag{9}$$

where C_j^{damage}, $C_j^{content}$, $C_j^{relocation}$, $C_j^{economic}$, C_j^{injury} and $C_j^{fatality}$ represent the damage repair cost, building appurtenances loss cost, relocation cost, rental income loss, medical expenses for minor and major casualties, and fatality cost, respectively, and P_j can be obtained from the performance-based fragility curves (Figure 9).

4.2. Assessment of Economic Losses

Through calculation, the total floor area of the SFVD was determined to be 280 m^2, and according to Reference [18], the initial cost of the SFVD was estimated to be about 0.812 million. According to the population density definition in ATC-13 [34], the occupancy rate is 4 persons per 1000 square feet (approximately 92.9 m^2). The total floor area yields an estimated occupancy of approximately 13 individuals. Regional variations introduce significant uncertainty in assessing seismic economic losses. Given the building's location in the Los Angeles area, the basic cost data from the Los Angeles region were referenced for this evaluation, as shown in Table 3.

Table 3. Value of basic loss and calculation formula in the damaged state.

Categories	Cost Value	Calculation Formula [35]
Demolition	USD 404.9/m^2	USD 404.9/m^2 × Total area × Damage factor
Contents costs	USD 875.4/m^2	USD 875.4/m^2 × Total area × Damage factor
Relocation	USD 49.0/month/m^2	USD 49.0/month/m^2 × Total area × Loss of function
Rental loss	USD 17.94/month/m^2	USD 17.94/month/m^2 × Total area × Loss of function
Income loss	USD 252.6/month/m^2	USD 252.6/month/m^2 × Total area × Loss of function
Minor injury	USD 2600/person	USD 2600/person × Occupancy × Minor injury
Serious injury	USD 26,000/person	USD 26,000/person × Occupancy × Serious injury
Human death	USD 4,758,000/life	USD 4,758,000/life × Occupancy × Fatality

It should be noted that this cost data corresponds to 2019 values, and their current value needs to be adjusted using an annual growth rate. According to the International Construction Market Survey 2018 [36], which reported an average annual growth rate of 5% over the past three years in Los Angeles, the following conversion formula was proposed:

$$C_{2025} = C_{2019}(1 + 0.05)^6 \tag{10}$$

To calculate the economic losses of the SFVD at various damage states, the loss assessment methodology from Reference [18] was adopted. This methodology, which utilizes damage probability matrices, was determined by ATC-13 [34] and FEMA-227 [37] for seismic damage and loss assessment of multiple types of buildings. The details are shown in Table 4, which defines the corresponding inter-story drift ratio for various damage states and gives the associated damage factors, loss of function days, minor injury rates, serious injury rates, and fatality rates.

Table 4. Definitions of damage states and loss indices.

Performance Level	Story Drift Ratio (%)	Damage Factor	Loss of Function (d)	Minor Injury (%)	Serious Injury (%)	Fatality (%)
I	$\theta < 0.2$	0.0	0	0	0	0
II	$0.2 < \theta < 0.4$	0.005	3.4	0.003	0.0004	0.0001
III	$0.4 < \theta < 0.7$	0.05	12.08	0.03	0.004	0.001
IV	$0.7 < \theta < 1.5$	0.2	44.72	0.3	0.04	0.01
V	$1.5 < \theta < 2.5$	0.45	125.66	3	0.4	0.1
VI	$2.5 < \theta < 5.0$	0.8	234.76	30	4	1
VII	$5.0 < \theta$	1.0	346.93	40	40	2

According to the cost data and loss indices in Tables 3 and 4, as well as Equations (7)–(10), the economic losses for various seismic intensities can be calculated, as shown in Figure 11. The results show that economic losses increase gradually with increasing corrosion time. However, the influence of corrosion time on the losses is not significant. The loss difference between the SFVDs with 0 days and 192 days of corrosion reaches a maximum value of USD 103,582 when the $S_a(T_1)$ is 3.26 g, which is about 9.52% of the initial cost. Notably, under relatively strong or weak seismic intensities, the economic loss curves of SFVDs at different corrosion times exhibit significant overlap. In addition, early-stage corrosion has a more pronounced impact on economic losses. Hence, it should be feasible for builders to transform economic losses from corrosion into prevention investments through systematic risk conversion.

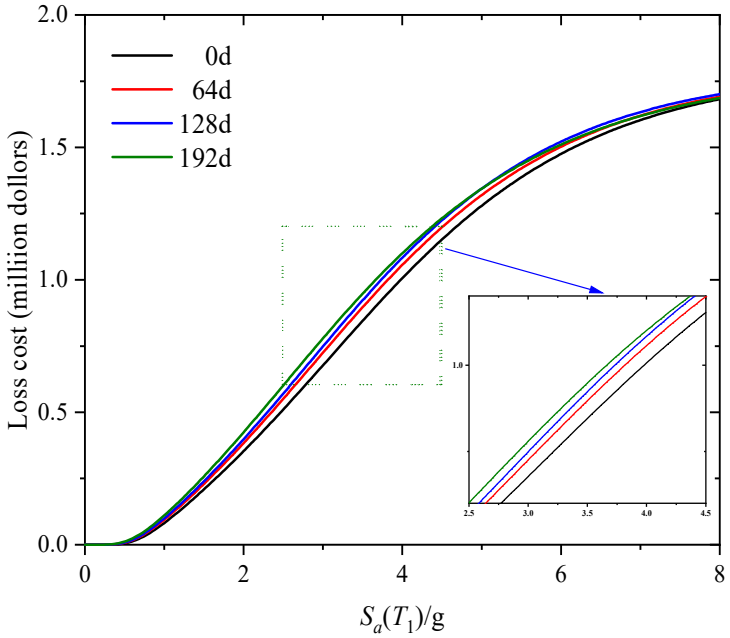


Figure 11. Economic losses for various corrosion times.

5. Conclusions

In this paper, a salt spray accelerated corrosion test was performed on Q355 steel, followed by tensile tests to investigate the effects of corrosion on its mechanical properties. DIA was conducted to perform seismic fragility analysis on a 5-story SFVD at various corrosion times, and the economic losses were assessed. The main conclusions obtained are as follows:

1. With the increase of corrosion time, the mass loss rate and cross-section loss rate of steel gradually increase. Corrosion causes rust pits on the surface of steel, leading to a reduction in its effective cross-sectional area and thereby significantly lowering the mechanical property indices of steel, such as yield strength, ultimate tensile strength, and elongation. Although corrosion degrades the mechanical properties of steel, it does not affect its safety performance.
2. The probability of exceedance of the SFVD in the limit state increases gradually with increasing corrosion time. This effect is relatively minor in the IO and SD states, while it becomes significant in the CP state.
3. The economic losses of the SFVD increase with increasing corrosion time, with the maximum loss difference within the test seismic motion range being USD 103,582, which is about 9.52% of the initial cost. In addition, early-stage corrosion has a significantly pronounced impact on economic losses.

This study reveals the effects of corrosion on the seismic fragility and economic losses of steel frames and provides some preliminary results. Future research on the long-term behavior of steel frames should account for corrosion. In addition, the quantified results of the economic loss impact of corrosion indicate that transforming corrosion-induced economic losses into preventive investments, such as anti-corrosion coatings, should be feasible.

Author Contributions: Conceptualization, W.Q. and H.W.; methodology, H.W.; software, Z.Z. and W.L.; validation, C.G.; formal analysis, W.Q.; investigation, W.Q.; resources, W.Q.; data curation, W.Q.; writing—original draft preparation, W.Q.; writing—review and editing, W.Q. and H.W.; visualization, S.L.; supervision, W.Q.; project administration, W.Q.; funding acquisition, W.Q. All authors have read and agreed to the published version of the manuscript.

Funding: This research received no external funding.

Data Availability Statement: The raw data supporting the conclusions of this article will be made available by the authors on request.

Conflicts of Interest: The authors declare no conflicts of interest.

References

1. Gatheeshgar, P.; Poologanathan, K.; Gunalan, S.; Shyha, I.; Sherlock, P.; Rajanayagam, H.; Nagaratnam, B. Development of affordable steel-framed modular buildings for emergency situations (COVID-19). *Structures* **2021**, *31*, 862–875. [CrossRef]
2. Wasse, A.D.; Dai, K.; Wang, J.; Sharbati, R. State-of-the-art review: Seismic design and performance assessment of special concentrically braced frames developed for complex industrial building structures. *Int. Steel. Struct.* **2024**, *24*, 280–295. [CrossRef]
3. Pourzangbar, A.; Vaezi, M.; Mousavi, S.M.; Saber, A. Effects of brace-viscous damper system on the dynamic response of steel frames. *Int. J. Eng. Trans. B Appl.* **2020**, *33*, 720–731.
4. Zhou, C.; Wen, H.; Zhao, J.; Jiang, L.; Xu, X.; Zheng, H.; Tian, Y.; Liang, M.; Wang, X.; Zhang, H. Investigation of the Hysteresis Performance of Multi-Story Y-Shaped Eccentrically Bare Braced Steel Frame with Block Slit Damper (BSD). *Buildings* **2025**, *15*, 451. [CrossRef]
5. Zhao, X.; Liao, X.; Hu, Z.; Li, X.; Nie, Y.; Liu, J.; Xu, Y. Seismic fragility analysis of steel pipe pile wharves with random pitting corrosion. *Buildings* **2023**, *13*, 2619. [CrossRef]
6. Rajput, A.; Paik, J.K. Effects of naturally-progressed corrosion on the chemical and mechanical properties of structural steels. *Structures* **2021**, *29*, 2120–2138. [CrossRef]

7. Guo, Q.; Wu, Z.; Xing, Y.; Lu, Y.; Zhang, F.; Li, W. Corrosion evolution and mechanical property deterioration of Q355NH weathering steel in long-term neutral salt spray environment. *Constr. Build. Mater.* **2024**, *411*, 134193. [CrossRef]
8. Kong, Z.; Jin, Y.; Hossen, G.M.S.; Hong, S.; Wang, Y.; Vu, Q.; Truong, V.; Tao, Q.; Kim, S. Experimental and theoretical study on mechanical properties of mild steel after corrosion. *Ocean. Eng.* **2022**, *246*, 110652. [CrossRef]
9. Gkatzogiannis, S.; Weinert, J.; Engelhardt, I.; Knoedel, P.; Ummenhofer, T. Correlation of laboratory and real marine corrosion for the investigation of corrosion fatigue behaviour of steel components. *Int. J. Fatigue.* **2019**, *126*, 90–102. [CrossRef]
10. Wu, Q.; Chen, X.; Fan, Z.; Nie, D.; Wei, R. Corrosion fatigue behavior of FV520B steel in water and salt-spray environments. *Eng. Fail. Anal.* **2017**, *79*, 422–430. [CrossRef]
11. Wang, H.; Liu, X.; Xu, S.; Hu, S. Experimental investigation on seismic performance of CHS T-joints in salt spray environment. *J. Constr. Steel Res.* **2024**, *221*, 108910. [CrossRef]
12. Zhang, Y.; Fang, C.; Wang, W.; Wu, L.; Cao, P. Influence of corrosion on seismic performance of steel beam-to-column connections. *Eng. Struct.* **2024**, *312*, 118284. [CrossRef]
13. Zhang, X.; Zheng, S.; Zhao, X. Experimental and numerical study on seismic performance of corroded steel frames in chloride environment. *J. Constr. Steel Res.* **2020**, *171*, 106164. [CrossRef]
14. Zhang, X.; Zheng, S.; Zhao, X. Experimental and numerical investigations into seismic behavior of corroded steel frame beams and columns in offshore atmospheric environment. *J. Constr. Steel Res.* **2023**, *201*, 107757. [CrossRef]
15. Lad, D.; Freddi, F.; Ghosh, J.; Rossetto, T. Impact of corrosion deterioration on the seismic performance of steel frame structures. In Proceedings of the SECED 2023 Conference, Cambridge, UK, 14 September 2023.
16. Xu, S.; Zhang, Z.; Li, R.; Wei, L. A method for the seismic vulnerability assessment of corroded steel structures. *J. Eng. Mech.* **2018**, *35*, 107–115. (In Chinese)
17. Lekeufack, B.C.; Fu, B.; Samuel, M.A.; Alam, S. Seismic resilience assessment of coastal carbon and weathering steel moment frame considering uniform atmospheric corrosion effects. *Structures* **2024**, *69*, 107274. [CrossRef]
18. Jiang, L.; Jiang, L.; Hu, Y.; Ye, J.; Zheng, H. Seismic life-cycle cost assessment of steel frames equipped with steel panel walls. *Eng. Struct.* **2020**, *211*, 110399. [CrossRef]
19. *GB/T 228.1-2010*; Metallic Materials Tensile Testing Part 1: Method of Test Method at Room Temperature. China Standards Press: Beijing, China, 2010. (In Chinese)
20. *GB/T 3075-2008*; Metal Materials-Fatigue Testing Axial Force-Controlled Method. China Standards Press: Beijing, China, 2008. (In Chinese)
21. Aditya, P.A.; Navvar, K.M.; Bahubali, J.K.; Pandikkadavath, M.S.; Mangalathu, S. Near-fault seismic vulnerability assessment of corrosion inflicted steel moment resisting frames. *J. Constr Steel. Res.* **2025**, *229*, 109527. [CrossRef]
22. *GB/T 19879-2005*; Steel Plates for Building Structures. China Standards Press: Beijing, China, 2005. (In Chinese)
23. Chen, X.; Lin, Z. *Structural Nonlinear Analysis Program Opensees Theory and Tutorial*; China Architecture & Building Press: Beijing, China, 2014. (In Chinese)
24. Cornell, C.A.; Jalayer, F.; Hamburger, R.O.; Da, F. The probabilistic basis for the 2000 SAC/FEMA steel moment frame guidelines. Submitted to. *J. Struct. Eng.* **2002**, *128*, 526–533. [CrossRef]
25. Cheng, X.; Jiang, L.; Yang, J.; Zhang, X.; Hu, Y. Seismic performance and risk mitigation of CFS shear walls with CFRP-reinforced screw connections and special-shape L-section end studs. *J. Build. Eng.* **2024**, *88*, 108824. [CrossRef]
26. Ye, J.; Jiang, L. Seismic risk assessment of mid-rise cold-formed steel structures in China considering various uncertainties. *China Civ. Eng. J.* **2021**, *54*, 74–83. (In Chinese)
27. Jiang, L.; Ye, J. Quantifying the effects of various uncertainties on seismic risk assessment of CFS structures. *Bull. Earthq. Eng.* **2020**, *18*, 241–272. [CrossRef]
28. *GB 50011-2010*; Code for Seismic Design of Buildings. Architecture and Building Press: Beijing, China, 2016. (In Chinese)
29. FEMA356. *NEHRP Guidelines for the Seismic Rehabilitation of Buildings*; Federal Emergency Management Agency: Washington, DC, USA, 2002.
30. Jiang, L.; Ye, J. Risk-based overall seismic robustness assessment of cold-formed steel structures considering vulnerability and fragility. *Bull. Earthq. Eng.* **2022**, *20*, 7161–7184. [CrossRef]
31. Liu, Y.; Hu, Y.; Zhao, J.; Jiang, L.; Sun, H.; Wang, D. Seismic risk mitigation of concrete-filled double-skin steel tube frames with beam-only-connected shear walls. *Structures* **2025**, *71*, 107949. [CrossRef]
32. Silva, A.; Macedo, L.; Monteiro, R.; Castro, J.M. Earthquake-induced loss assessment of steel buildings designed to Eurocode 8. *Eng. Struct.* **2020**, *208*, 110244. [CrossRef]
33. Nettis, A.; Di Mucci, V.M.; Ruggieri, S.; Uva, G. Seismic fragility and risk assessment of isolated bridges subjected to pre-existing ground displacements. *Soil. Dyn. Earthq. Eng.* **2025**, *194*, 109335. [CrossRef]
34. ATC-13. *Earthquake Damage Evaluation Data for California*; Applied Technology Council: Redwood City, CA, USA, 1985.
35. Zhu, J.; Zhao, J.; Tan, P.; Zhou, F. Seismic life-cycle loss estimation of single-story factory buildings. *Earthq. Eng. Eng. Dyn.* **2018**, *38*, 51–64. (In Chinese)

36. Turner & Townsend and Federal Emergency Management Agency (FEMA). *International Construction Cost Survey 2018–2019*; Turner & Townsend: Mumbai, India, 2018.
37. FEMA 227. *A Benefit-Cost Model for the Seismic Rehabilitation of Building*; Federal Emergency Management Agency: Washington, DC, USA, 1992; Volume 1.

Disclaimer/Publisher's Note: The statements, opinions and data contained in all publications are solely those of the individual author(s) and contributor(s) and not of MDPI and/or the editor(s). MDPI and/or the editor(s) disclaim responsibility for any injury to people or property resulting from any ideas, methods, instructions or products referred to in the content.